

Time-Domain Multistatic Radar System for Microwave Breast Screening

Emily Porter, Evgeny Kirshin, Adam Santorelli, *Student Members, IEEE*
Mark Coates and Milica Popović, *Senior Members, IEEE*

Abstract—This paper presents an experimental system for microwave breast cancer detection that uses multistatic radar. The system operates by transmitting a short-duration pulse and collecting the signals scattered within the breast. We describe the 16-element array, along with the pulse generation scheme, switches and all auxiliary equipment. This work provides a sample selection of the collected time-domain data, and shows the proof of concept by imaging the breast tumors in realistically shaped breast phantoms.

Index Terms—Biomedical imaging, cancer detection, microwave imaging, multistatic radar.

I. INTRODUCTION

THIS work presents an experimental time-domain microwave breast cancer detection system validated using breast phantoms with realistic shape, size and composition. Microwave methods offer a promising imaging modality for breast monitoring due to lower cost than magnetic resonance imaging (MRI). Further, unlike mammography, they can be made to be relatively comfortable for the patient, with no ionizing radiation.

Experimental microwave breast imaging systems operating in the frequency-domain have been widely published, for example in [1] – [5], yet few time-domain measurement systems have been fully developed [6], [7], [8]. To the best of our knowledge, existing systems that record in the time-domain have undergone basic testing relative to their counterpart frequency-domain systems, with only numerical simulations [9], unrealistically shaped [8] and sized breast phantoms [6], [10], or designs and testing that are not well adapted to clinical studies [7], [10]. One particularly advanced study presented time-domain measurements on cylindrical phantoms with various tissue compositions, with mixed results [8]. In general, time-domain approaches could offer advantages over frequency-domain methods in terms of decreased signal processing, higher scan speeds, and cost-

effectiveness, with the trade-off of lower signal-to-noise ratio [6]. Systems utilizing frequency-domain measurements are simpler, usually requiring a vector network analyzer and no separate pulse generation and signal-recording equipment. Nonetheless, due to advantages that both time- and frequency-domain measurement systems possess, each is a worthwhile avenue of thorough investigation in the quest for an optimal microwave breast cancer detection system.

In our past work [7], we examined the feasibility of an early-stage experimental system, consisting of two antennas, for time-domain breast cancer detection. In this work, we present a system operating with a complete, sixteen-element antenna array. The array is composed of travelling-wave tapered and loaded transmission-line antennas (TWTLTAs) [11], and allows for recording of both co-polarized and cross-polarized responses. We show here, for the first time, operation of our system with the recording of full sets of multistatic signals and the generation of corresponding breast images. In this work, we focus our investigation on the measurement system itself, the output signals of which are processed with a well-tested image-formation algorithm, described in [12]. This research represents progress in time-domain measurement methods for breast cancer detection, as we demonstrate for the first time successful imaging of realistically shaped and sized breast models.

In the next two sections, we describe the components of the system and the test scenarios investigated. We then demonstrate the system’s functionality by producing images of tumors embedded within breast phantoms.

II. TIME-DOMAIN BREAST IMAGING SYSTEM

A. Overview

The goal of our breast imaging system is to detect cancerous tumors at their early stage when treatment of the disease has the highest chance of success. The system would do so by frequent monitoring of the breast tissue. Patients would undergo a microwave breast scan after they are proclaimed to be cancer-free using a pre-determined standard method. The scan is then repeated at regular intervals (at the same time with respect to the menstrual cycle) and is automatically compared to previous scan results to identify potential developing malignant growths. Following such identification, the tumor’s presence can be confirmed and staged using standard modalities such as mammography or magnetic resonance imaging. Breast monitoring through

Manuscript received January 17, 2013, revised February 12, 2013. This work was supported by the Natural Sciences and Engineering Research Council of Canada (NSERC), le Fonds québécois de la recherche sur la nature et les technologies (FQRNT) and Partenariat de Recherche Orientée en Microélectronique, Photonique et Télécommunications (PROMPT).

The authors are with the Department of Electrical and Computer Engineering, McGill University, Montreal QC H3A 0E9, Canada (email: {emily.porter, evgeny.kirshin, adam.santorelli}@mail.mcgill.ca, {mark.coates, milica.popovich}@mcgill.ca).

comparison of past and current scans was demonstrated numerically with good results in [9].

B. Experimental Setup

The breast imaging system contains several components. A key component is the radome; it is the interface between the system and the breast. The radome, in which the breast is placed, is a hemispherical dielectric bowl, with its exterior surface containing slots that house the 16 antennas. The system operates in time-domain: a short-duration generic pulse is re-shaped for the desired frequency content; then, it is fed to the antenna array; the emitted microwave pulse scatters within the breast and the signals collected by the antennas are recorded by an oscilloscope.

A schematic of the system is shown in Fig. 1. The transmitting circuitry consists of an off-the-shelf pulse generator that produces pulses with full-width at half-maximum duration of 70 ps, triggered at a rate of 25 MHz. This generic impulse is reshaped by a synthesized broadband reflector (SBR), a cost-effective planar microstrip line in which a varying conductive line width is used to produce a desired frequency response [13]. The SBR reshapes the pulse (initially containing significant power below 1 GHz) to limit its frequency content to the 2 - 4 GHz range, which is the range identified as optimal for our microwave detection system [14]. The SBR is a reflection mode 2-port device; the first port connects to a directional coupler and acts as both the input and output port whereas the second port is terminated with a 50- Ω broadband load. The directional coupler is used to route the pulse between the generator, the SBR, and the amplifier (2 - 8 GHz operating range, +35 dB gain, maximum output power 33 dBm). This amplification phase is needed to increase the power transmitted into the breast, which is inherently low due to the following factors: low output power of generic pulse generator, inherent SBR losses, and losses from the directional coupler and cables required for the transmitting circuitry. From the amplifier, the pulse is fed into an antenna that is held in the radome and propagates into the breast.

The receiving circuitry consists of a switching network, which selects each of the antennas in turn, and an oscilloscope that records the received signal, i.e., the signal scattered within the breast. Of the 16 antennas, one transmits at a time and the other 15 receive in turn. The process is repeated for each antenna acting as transmitter. This results in a total of 240 signals for the complete data set. A photograph of the system showing the radome and antenna array is given in Fig. 2.

III. TEST METHODOLOGY

A. Breast Phantoms

The models used to test our system are shaped and sized as a typical B-cup breast. They contain distinct fat, skin and tumor phantoms each approximating the dielectric properties of the corresponding breast tissues over the microwave frequency range of interest. A description of how the tissue phantoms are made, along with measurements of their

dielectric properties can be found in [15]. The realistically shaped phantoms measure 17.5 cm x 16.5 cm at maximum cross-section, with a height of up to 8 cm. They are composed of an uneven, textured skin layer (average thickness 2 mm) filled with fat mimicking-material and tumor(s) of given shape/size placed at any desired location. Photographs of the complete, realistically shaped phantoms are provided in Fig. 3.

B. Test Scenario

To perform test measurements on breast phantoms, we place a given phantom into the radome surrounded by a thin layer of ultrasound gel. The ultrasound gel fills the air gaps between the breast surface and the radome and provides a lossy medium at microwave frequencies that suppresses transmission and reflection of signals not passing directly through the phantom. Ultrasound gel is chosen for use as the breast immersion medium because of its favorable electrical and mechanical properties: it is lossy, so it attenuates unwanted multiple reflections between the skin and the radome wall, and it conforms well to the breast shape without the spill risk of a liquid. Ultrasound gel is also already approved for medical use and is thus readily available to hospitals and clinics.

The tumors are placed at known locations within the phantoms. Two full sets of multistatic signals are recorded for each phantom: one with only healthy tissues present in the phantom and a second after the tumor has been inserted. This is intended to mimic the patient having multiple breast scans and, over the time in between them, developing a cancerous lesion. The portion of scattered signals attributed to the tumor's presence is obtained using a simplified approach to that demonstrated in [9]; one that compares past and current data sets. Our procedure time-aligns data from the two sets and normalizes the corresponding signals from the same antenna-pairs in order to remove the direct pulse. We then eliminate signals any that are of poor quality (close to or at the noise level), and compare the remaining equivalent signals from each of the two data sets. The output signals from this series of operations are then the basis for the applied imaging algorithm. This method allows for demonstrating the system's functionality without it relying on the abilities of advanced signal processing and imaging algorithms.

Two different breast phantoms are examined in this work. Each phantom contains a roughly spherical tumor with a radius of less than 1 cm. We chose this tumor size based on medical practice, as these dimensions represent the limiting case for *Stage 1* breast cancer [16], an optimal stage for detection and successful treatment. In the first phantom the tumor is placed in the left half of the breast (position "A"), whereas in the second phantom the tumor is located in the right half of the breast ("B"). The tumors are centered at depths between 1 cm and 3 cm above the chest wall.

Since we aim to focus our present investigation on our measurement system, we apply an imaging method that is already well known in the literature. Images are generated

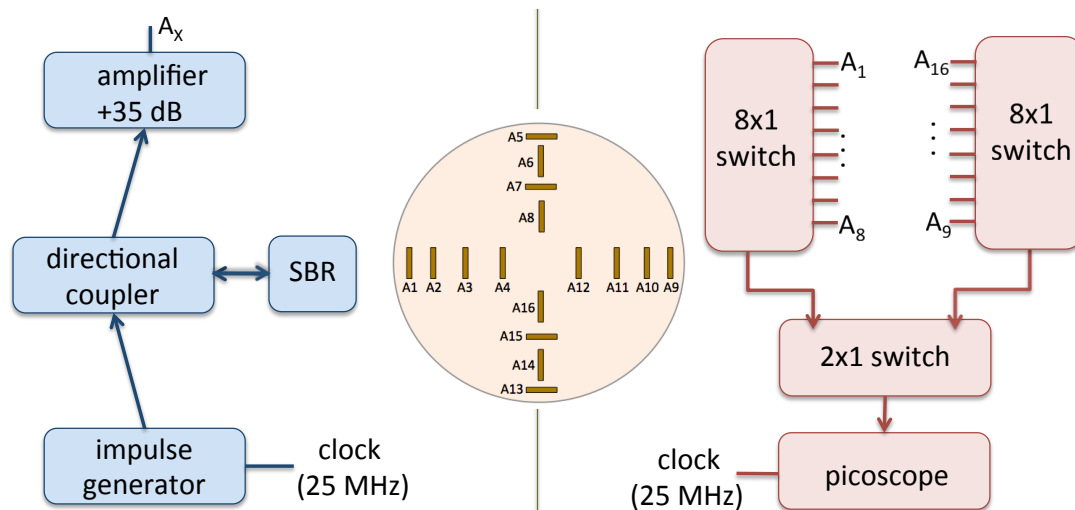


Fig. 1. Schematic diagram of the time-domain breast imaging system (transmitting circuitry on the left; radome and antennas in the center; receiving circuitry on the right). A_x can be any transmitting antenna ($x = 1:16$).

using the Delay-Multiply-and-Sum (DMAS) algorithm [12]. Although not specifically adapted to our system and hence perhaps not optimal from an imaging point-of-view, it allows us to easily examine the functionality of our detection prototype.

IV. RESULTS AND DISCUSSION

Coronal slices from images generated using the collected signals with tumors in Positions A and B are shown in Figs. 4 and 5, respectively. Within the images, dark red highlights strongly scattered electromagnetic energy, whereas blue indicates less scattering; we also note that the energy is plotted on a linear scale. The images are normalized to the global maximum intensity value of each reconstructed data set. This global maximum intensity value represents the location of the most prominent EM scatterer, which should be the embedded tumor, and is denoted in the normalized images by the darkest red color. The global maximum is the maximum value across the entire 3-D domain; it is not just the maximum of a single 2-D coronal slice. In both Figs. 4 and 5, the maximum scattered energy occurs at the tumor location - indicating that the largest scatterer found in the breast by the algorithm is indeed the tumor.



Fig. 2. Photograph of the radome and antenna array.



Fig. 3. Photographs of the realistically shaped breast phantoms.

Table I summarizes key imaging parameters: the signal-to-clutter ratio (SCR, the ratio between the scattered intensity at the tumor location and the next highest intensity) and the tumor localization error (the distance between where the center of the tumor actually is and where the global maximum in the images is found to be). The localization error is shown in the two coronal planes (y, z); the error in the x -dimension is not shown as for both Positions A and B the maximum scatterer in the images is found to be within the same depth region as where the tumor is actually located. We note, however, that the localization error is not an exact metric as the tumor is placed by hand and its location is therefore not precisely controlled.

From observing the parameters in Table I, it is clear that the tumors are easily detected in both positions. The average localization errors are 7 mm and 11 mm in the z - and y -dimensions, respectively. The localization error could be improved by increasing the number of antennas in the array, distributing the sensors evenly around the radome, and through imaging algorithms that include the dispersive nature of breast tissues. It is of interest to compare the SCRs found in our work with those presented in the literature; however, such a comparison is not straightforward as the SCR is affected by many other factors. For instance, breast size, shape, and composition, tissue contrast, tumor size, applied imaging algorithm, and the components of the measurement system all impact the SCR. In [8], the SCR with time-domain measurements was reported to be between 0.23 dB and 1.63 dB (depending on the method used) for a 4-mm tumor embedded in a cylindrical, homogeneous fatty phantom; whereas in [17] the SCR with frequency-domain measurements on a 6-mm tumor in a hemispherical, homogeneous fatty phantom was between 3.8 dB and 8.2 dB, varying with the tumor location and imaging method used. Despite the varying factors, the SCR obtained with our system is within the range of those achieved in other systems under similar conditions. Ongoing work includes heterogeneous

phantoms, in order to identify the imaging obstacles introduced by complex human tissue structure.

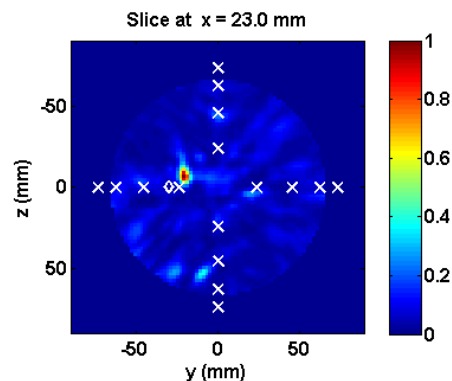


Fig. 4. Image of a breast phantom with a tumor in position A. The “x” markers represent the positions of the antennas, and the diamond marks the actual location of the tumor center. Slice depth $x = 23$ mm is from the chest wall.

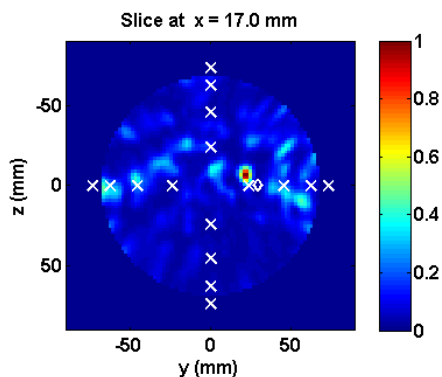


Fig. 5. Image of a breast phantom with a tumor in position B. The “x” markers represent the positions of the antennas, and the diamond marks the actual location of the tumor center. Slice depth $x = 17$ mm is from the chest wall.

TABLE I

SUMMARY OF IMAGE PARAMETERS FOR TUMORS IN POSITIONS A AND B: SIGNAL-TO-CLUTTER RATIO (SCR) AND TUMOR LOCALIZATION ERROR

	Position A	Position B
SCR (dB)	8.2	6.8
Error (y, z) (mm)	(9, 7)	(13, 7)

V. CONCLUSION

This work has demonstrated a functional time-domain microwave breast cancer imaging system. We describe the experimental system and show via reconstructed breast images that, for the first time using a time-domain measurement system, tumors in life-like breast phantoms can be successfully located. The images show a good signal-to-clutter ratio and clearly localize the tumors. Near-future work includes the adaptation of imaging algorithms to our specific system (e.g. incorporation of antenna properties, adaptive assessments of the data being monitored), as well as testing through more complex scenarios.

ACKNOWLEDGMENT

The authors would like to thank J. Gauthier at Polytechnique Montreal for fabricating the antennas. We are grateful to McGill University undergraduates, M. Lee and R. Brais, for their help with breast phantom fabrication.

REFERENCES

- [1] M. Klemm, J. Leendertz, D. Gibbins, I. J. Craddock, A. W. Preece, and R. Benjamin, “Microwave radar-based differential breast cancer imaging: imaging in homogeneous breast phantoms and low contrast scenarios,” *IEEE Trans. Antennas Propag.*, vol. 58, no. 7, July 2010.
- [2] A. Golnabi, P. M. Meaney, S. Geimer, and K. D. Paulsen, “Microwave imaging for breast cancer detection and therapy monitoring,” *Biomedical Wireless Technologies, Networks, and Sensing Systems (BioWireless)*, 2011 *IEEE Topical Conference on*, pp. 59–62, Jan. 2011.
- [3] T. Grzegorzczak, P. M. Meaney, P. Kaufman, R. diFlorio-Alexander, and K. D. Paulsen, “Fast 3-D tomographic microwave imaging for breast cancer detection,” *IEEE Trans. Med. Imag.*, vol. 31, no. 8, Aug. 2012.
- [4] J. Bourqui, J. M. Sill, and E. C. Fear, “A prototype system for measuring microwave frequency reflections from the breast,” *Int. J. Biomedical Imaging*, vol. 2012, 2012.
- [5] X. Li, E. J. Bond, B. D. V. Veen, and S. C. Hagness, “An overview of ultra-wideband microwave imaging via space-time beamforming for early-stage breast-cancer detection,” *IEEE Antennas Propag. Mag.*, vol. 47, no. 1, pp. 19–34, Feb. 2005.
- [6] X. Zeng, A. Fhager, P. Linner, M. Persson, and H. Zirath, “Experimental investigation of the accuracy of an ultrawideband time-domain microwave-tomographic system,” *IEEE Trans. Instrum. Meas.*, vol. 60, no. 12, Dec. 2011.
- [7] E. Porter, A. Santorelli, M. Coates, and M. Popović, “Time-domain microwave breast cancer detection: extensive system testing with phantoms,” *Technol Cancer Res Treat.*, vol. 12, pp. 131–143, 2013.
- [8] J. C. Y. Lai, C. B. Soh, E. Gunawan, and K. S. Low, “UWB microwave imaging for breast cancer detection – experiments with heterogeneous breast phantoms,” *Prog. Electromagn. Res. M*, vol. 16, pp. 19–29, 2011.
- [9] D. Byrne, M. O’Halloran, M. Glavin, and E. Jones, “Breast cancer detection based on differential ultrawideband microwave radar,” *Prog. Electromagn. Res.*, vol. 20, pp. 231 – 242, 2011.
- [10] W. Liu, H. M. Jafari, S. Hranilovic, and M. J. Deen, “Time domain analysis of UWB breast cancer detection,” *Communications, 2006 23rd Biennial Symposium on*, pp. 336 – 339, Kingston, Canada, May 30 – June 1, 2006.
- [11] H. Kanj, and M. Popović, “A novel ultra-compact broadband antenna for microwave breast tumor detection,” *Prog. Electromagn. Res.*, vol. 86, pp. 169–198, 2008.
- [12] H. Been Lim, N. Thi Tuyet Nhung, E. P. Li, and N. Duc Thang, “Confocal microwave imaging for breast cancer detection: Delay-Multiply-and-Sum image reconstruction algorithm,” *IEEE Trans. Biomed. Eng.*, vol. 55, no. 6, pp. 1697–1704, June 2008.
- [13] I. Arnedo, J. D. Schwartz, M. A. G. Laso, T. Lopetegui, D. V. Plant, and J. Azaa, “Passive microwave planar circuits for arbitrary UWB pulse shaping,” *IEEE Microw. Wireless Compon. Lett.*, vol. 18, no. 7, pp. 452–454, July 2008.
- [14] E. Porter, A. Santorelli, S. Winkler, M. Coates, and M. Popović, “Time-domain microwave cancer screening: optimized pulse shaping applied to realistically shaped breast phantoms,” *Microwave Symposium Digest (MTT), 2012 IEEE MTT-S International*, Montréal, Canada, pp. 1 – 3, June 17 – 22, 2012.
- [15] A. Santorelli, “Breast screening with custom-shaped pulsed microwaves,” *M. Eng. Thesis, Dept. Elec. and Comp. Eng., McGill Univ.*, Montréal, Canada, 2012.
- [16] Canadian Cancer Society. *Staging and grading for breast cancer*. [Online]. Available: www.cancer.ca
- [17] M. Klemm, I. J. Craddock, J. Leendertz, A. Preece, and R. Benjamin, “Radar-based breast cancer detection using a hemispherical antenna array – experimental results,” *IEEE Trans. Antennas Propag.*, vol. 57, no. 6, June 2009.